Terahertz on-chip sensing by exciting higher radial order spoof localized surface plasmons

Applied Physics Express 13, 012014 (2020) LETTER
https://doi.org/10.7567/1882-0786/ab5eb3

Terahertz on-chip sensing by exciting higher radial order spoof localized surface plasmons

Ji Zhou[1], Lin Chen[1,2*], Qingyun Sun[1], Denggao Liao[1], Li Ding[1], Alexey V. Balakin[3], Alexander P. Shkurinov[3], Jingya Xie[1], Xiaofei Zang[1], Qingqing Cheng[1], and Yiming Zhu[1*]

[1]Shanghai Key Lab of Modern Optical System, University of Shanghai for Science and Technology, Shanghai 200093, People's Republic of China
[2]Shanghai Institute of Intelligent Science and Technology, Tongji University, Shanghai 200092, People's Republic of China
[3]Department of Physics and International Laser Center, Lomonosov Moscow State University, Leninskie Gory 1, Moscow 19991 Russia, ILIT RAS—Branch of the FSRC << Crystallography and Photonics >> RAS, Svyatoozerskaya 1, 140700, Shatura, Moscow Region, Russia

*E-mail: linchen@usst.edu.cn; ymzhu@usst.edu.cn

Received October 31, 2019; revised November 29, 2019; accepted December 4, 2019; published online December 24, 2019

We demonstrate higher radial order spoof localized surface plasmon (LSP) resonances excited by a planar plasmonic waveguide with a ladder-shaped unit as a unique platform for terahertz (THz) on-chip sensing. The frequency shifts induced by the different dielectric permittivities of edible oils for higher radial order spoof LSPs are more sensitive than those for the fundamental mode. Experimental and simulated results agree well with each other. The proposed structure is easily integrated and have potential applications in enhanced on-chip THz sensing.

Surface plasmon polaritons (SPPs), by their very nature, are propagating electromagnetic (EM) waves that can be confined at metal–dielectric interfaces which have two opposite permittivities.[1,2] Surface plasmons including SPPs and localized surface plasmons (LSPs) show a weakly localized capacity of EM waves near metallic surfaces at lower frequencies due to the fact that metal is regarded as a perfect electric conductor.[3] Furthermore, spoof SPPs/LSPs were introduced by using structured metallic surfaces to mimic natural properties in microwave and terahertz (THz) frequencies.[4–6] The spoof SPP structure has a lower effective surface plasma frequency and can be controlled by adjusting its geometry on designed surfaces. Several periodic designed surface structures with different shapes were proposed to excite spoof SPPs.[7,8] In the case of spoof LSPs, changing the shape and dimensions of metallic disks can also have a tremendous impact on the multipolar modes of spoof LSPs,[9–14] which originate from excitations of conduction electrons on subwavelength metallic particles. Such spoof SPPs/LSPs have been applied in a broad range of technological areas, such as optical antennas and sensors.[15–19]

The behavior of higher-order modes of spoof SPPs has also been widely studied. These higher-order modes can be excited on the geometry of deep-corrugated metal surfaces and are more sensitive to the surrounding environment.[20–23] Similarly, higher radial order spoof LSP modes have been observed at microwave frequencies.[12] However, there are several limitations on previous structures that can excite higher (radial) order modes of spoof SPPs (LSPs) for actual application. In Ref. 21, an optical prism is shown not to be beneficial for integration. In terms of higher radial order spoof LSPs, a single meta-atom has been excited by microwave probes, which is not easily extended to the THz range in experiments.[12]

In this work, we propose an on-chip method to excite higher radial order spoof LSPs at THz frequencies. The THz band (the lower and upper frequency limits are each put at 100 GHz and 10 THz) has many attractive characteristics. For instance, THz waves are non-ionizing and can penetrate materials composed of non-polar molecules (such as oil).[18] When a commercial THz time-domain spectrometer is used to detect samples, the system requires a large volume of the sample and cannot be used for microsample testing.[18] Moreover, metasurfaces can strengthen the interaction between the substance and THz wave because of its strong electric field limitation.[13,14] However, the incident direction of the EM wave is not parallel to the surface of the chip which is not conducive to integration in practical applications.[24,25] Here, an on-chip THz sensor by coupling high radial order spoof LSPs with a planar plasmonic waveguide[26] is proposed. We find that the higher the radial mode is, the higher the sensitivity is. The dispersion relationships of three radial order modes are discussed. Frequency shifts due to the refractive index difference between edible oils and air are also found for the three radial order modes. The sensitivity of the second and third radial modes is 45.64 GHz/RIU and 25.35 GHz/RIU, respectively, which are higher than the fundamental mode. Experimental results show that highly sensitive detection of different edible oils can be achieved based on the refractive index differences of different types of edible oils. These results open a new door for the highly sensitive on-chip detection and integration of spoof LSPs based on higher radial order modes.

To excite higher radial order modes, a subwavelength deep-grooved corrugated metallic disk resonator (CMDR) is designed and coupled with an ultrathin planar spoof SPP waveguide. Figures 1(a) and 1(b) show the plasmonic sensing chip. The coplanar waveguide (CPW) port 1/2 can be used as the signal input/output port. The parameters of the CPW system are as follows: the width of the waveguide port w (30 μm), the width of slot lines g (2.82 μm) and the permittivity ε of the quartz substrate (3.75). In addition, by setting a ladder-shaped metallic unit with $H = 180$ μm, we realize field enhancement at the top of the ladder shape, which can act as a probe to excite a higher radial order of the CMDR with $R = 860$ μm, $r = 25$ μm, $d = 270$ μm, $a = 0.5d$, and $N = 20$ (the total number of grooves). The spacing between the spoof SPP part and the CMDR is 1.5 μm.

At first, we consider the metals as perfect electric conductors and analyze the dispersion relation of the CMDR which can support the propagation of spoof LSP waves along the corrugation grooves in a perfect conductor. The eigenvalue equation of the CMDR can be roughly expressed as:[21]

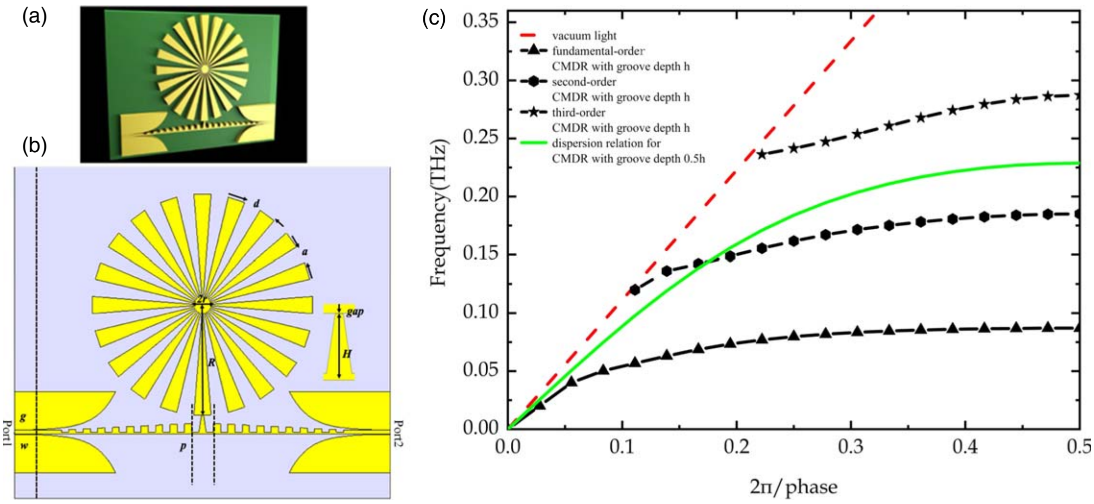

Fig. 1. (Color online) The designed plasmonic sensing chip. (a) The 3D side view and (b) the front view of the plasmonic sensing chip. (c) The dispersion relation of the CMDR with different groove depths.

$$\cot\left[k_0(R-r)\right] = \frac{a}{d}\sum_n \frac{k_0}{q_z^{(n)}} s_n^{\,2} \tag{1}$$

where $k_0 = w/c$ is the wave number in free space, c is the light velocity in vacuum, λ is the working wavelength, a is the width of the grooves of the CMDR, $h = R\text{–}r$ is the depth, d is the lattice constant, $q_z^{(n)} = \sqrt{(k_x^{(n)})^2 - k_0^{\,2}}$, and $s_n = \sin c(k_x^n w/2)$ (k_x is the parallel momentum). Considering the subwavelength approximation ($k_x > k_0$, $\lambda \gg a$, $\lambda \gg d$), the dispersion relation for TM polarization (E_x, E_z and H_y) propagating along the x direction can be obtained as

$$k_x = k_0\sqrt{1 + \frac{a^2}{d^2}\tan^2\left[k_0(R-r)\right]}\,. \tag{2}$$

According to Eq. (2), the frequency is mainly controlled by the depth of the groove h, and k_x is roughly proportional to h. As is known, spoof LSPs can propagate more slowly but can be confined more tightly to the corrugated metal structure. When h is large enough, for instance, $h > md$ (integer m is the resonance order), a higher radial order of the spoof LSP can be supported; in contrast, when $h < d$, only the fundamental mode exists on the corrugated metal surface.

To further illustrate how the groove depth can influence the propagation property, we calculate the dispersion relations of the proposed CMDR by using CST software, as shown in Fig. 1(c). The red dashed line and the green line are the dispersions for vacuum light and the CMDR with a groove depth $h_1 = 0.3{*}h$, respectively. When the groove depth decreases to h_1 ($h_1 < d$), only the fundamental mode can be excited. As the groove depth increases to larger than three times d, the second and third radial order modes can obviously be seen (dot–dash line and star–dash line, respectively).

Figure 2 shows the transmission coefficient S_{21} and the near-field electric distribution of spoof LSP modes near the surface of the plasmonic waveguide/resonator hybrid chip by using CST Microwave Studio. The boundary conditions of the x, y, and z axes are set to be open. The z-component of the electric field is plotted within the x–y plane 0.004 mm above the disk upper surface to monitor the unique characteristics of the electric field of the CMDR. In Fig. 2, the blue (red) line is the transmission coefficient S_{21} of the plasmonic waveguide chip without (with) the deep-groove CMDR. The fundamental-order mode is evaluated at frequencies ranging from 30 to 90 GHz [Fig. 2(a)], presenting azimuthal multipolar resonance characteristics corresponding to fundamental dipolar, quadrupolar and hexapolar modes (marked 2, 4, and 6 in Fig. 2, respectively). Their electric field characteristics have been reported earlier based on theoretical and experimental studies.[11,12] The second radial order modes cover the frequency range from 120 to 200 GHz, which fits well the dispersion shown in Fig. 1(c). The electric fields indicate the node ring along the grooves, showing the characteristics of radial second-order modes. Hexapolar (2–6), octupolar (2–8), decapolar (2–10) and dodecapolar (2–12) modes are also found in the spectrum. Similarly, third radial order modes can be found at around 280 GHz. The electric field shows two node rings along the grooves. Azimuthal multipolar resonances corresponding to the dodecapolar to octadecapolar modes are also listed in Fig. 2. It is worth noting that higher radial order modes can be successfully excited by the plasmonic waveguide in this planar chip.

To demonstrate the sensitivity of the designed plasmonic chip, we introduce eight kinds of oil (rapeseed oil, sunflower oil, olive oil, coconut oil, pumpkin seed oil, hemp oil, linseed oil and rice bran oil; their refractive indices have been identified by Marie Tobolova[27]) to observe the sensitivity to frequency shifts, as shown in Fig. 3(a). In the radial fundamental mode, the stronger resonance peak is located at 54 GHz and its Q factor is 13. The azimuthal profile demonstrates that it is a quadrupolar mode. In the radial second-order modes, the deepest resonance peak is found at 166.5 GHz with a Q factor of 49. Observing the electric field, we find that it is in decapolar mode in the azimuthal direction and has a node along the groove in the radial direction. Finally, when the frequency reaches 280.5 GHz, we can see the most sensitive resonance peak with a high Q factor of 172. The electric field presents a hexadecapolar mode profile in the azimuthal direction and there are two nodes along the groove in the radial direction, indicating that they are the radial third-order modes.

In order to compare the sensitivity of the three radial order modes, we compare the frequency shifts by changing the refractive index to evaluate the sensitivity of the different radial orders. Taking the metallic loss into consideration,

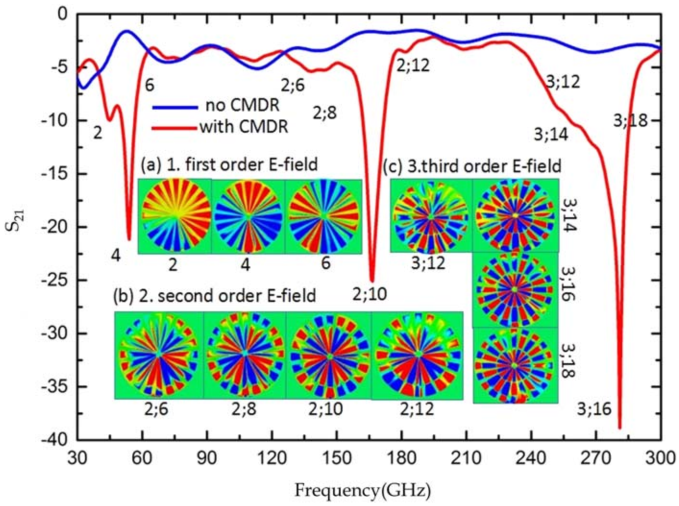

Fig. 2. (Color online) The S_{21} parameter of the sensing system and the electrical field of the CMDR at each position: (a) the radial fundamental-order modes; (b) the radial second-order modes; (c) the radial third-order modes.

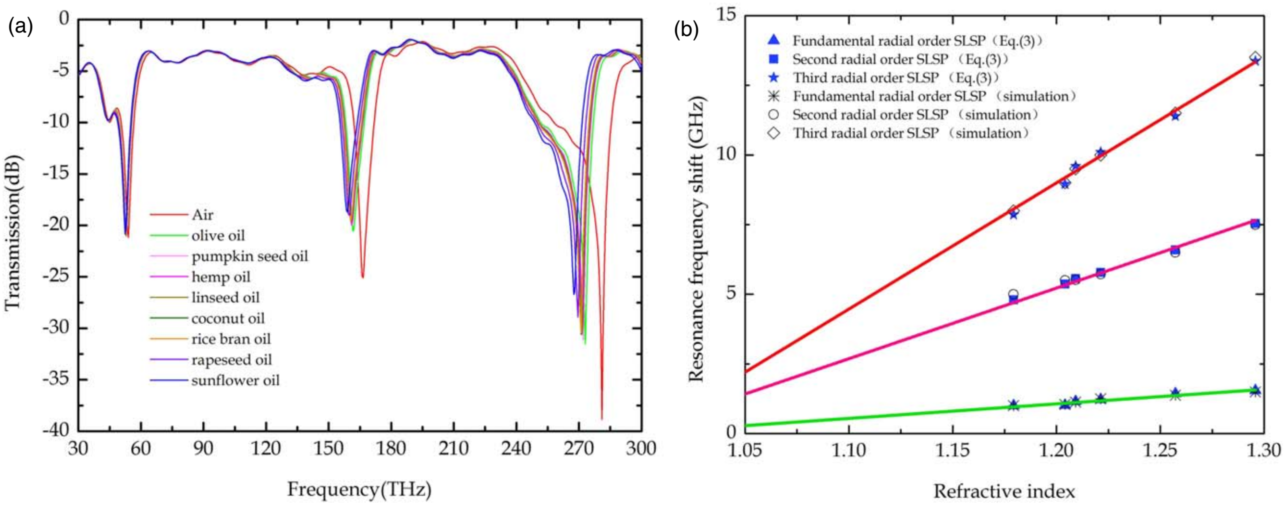

Fig. 3. (Color online) (a) Transmission spectra of three radial order modes with different edible oils and (b) the theoretical and simulated resonance frequency as a function of the filling refractive index n_d for different mode-based sensing. The solid points are the theoretical resonance frequency. The hollow points are the simulated resonance frequency. The lines are obtained by linear fitting of the simulation data.

when $k_0 n_d R \gg 1$, $k_0 n_d r \ll 1$ (a small core radius), the dispersion relation of higher radial order spoof LSPs can be expressed as:[12)]

$$k_{\rm spp} = k_d \sqrt{1 + \left(\frac{a}{d}\right)^2 \frac{\tan\left(k_d R - \frac{\pi}{4}\right) - \frac{\pi}{4}(k_d r)^2}{1 + \frac{\pi}{4}(k_d r)^2 \tan\left(k_d R - \frac{\pi}{4}\right)}} \tag{3}$$

where

$$k_d = k_0 n_d (1 + l_{\rm s}(i+1)/a)^{1/2}. \tag{4}$$

Here n_d is the refractive index of the medium filling the grooves and $l_{\rm s} = (k_0 {\rm Re}\sqrt{-\varepsilon_{\rm m}})^{-1}$ is the skin depth of the metal ($\varepsilon_{\rm m}$ is the complex permittivity of the metal film). Figure 3(b) plots the theoretical [according to Eq. (3)] and simulated resonance frequency shift [according to Fig. 3(a)] with respect to the refractive index n_d of the edible oil. The theoretical resonance frequencies according to Eq. (3) fit well the simulated results. This linear relationship can also be confirmed by Ref. 20. The resonance frequencies of all three order modes contain a linear relationship as a function of the refractive index n_d. A higher order has a bigger gradient—in other words, a higher sensitivity. The fitting lines for the different modes are $\Delta f_1 = -5.19 + 5.07 n_d$ (fundamental mode), $\Delta f_2 = -25.20 + 25.35 n_d$ (second-order radial mode), and $\Delta f_3 = -45.36 + 45.64 n_d$ (third-order radial mode). It is interesting that the sensitivity is roughly proportional to the fundamental-order modes. For example, in the situation of the third-order mode, the sensitivity (45.64 GHz/RIU) is nearly nine times that of the fundamental mode (5.07 GHz/RIU); at the same time, that of the second order (25.35 GHz/RIU) is exactly five times that of the fundamental mode. There is no doubt that a higher mode has a higher sensitivity to environment changes.

We also change the shape of the SPP part of the plasmonic chip to find out the function of the ladder-shaped unit by comparing the transmission coefficients S_{21} with the normal shape [Fig. 4(a)] and with the ladder shape [Fig. 4(b)]. Compared to the normal shape, near the CMDR, we set a ladder-shaped metallic unit with $H = 180\ \mu$m to make a sudden change in this guiding structure. In Fig. 4(c), by

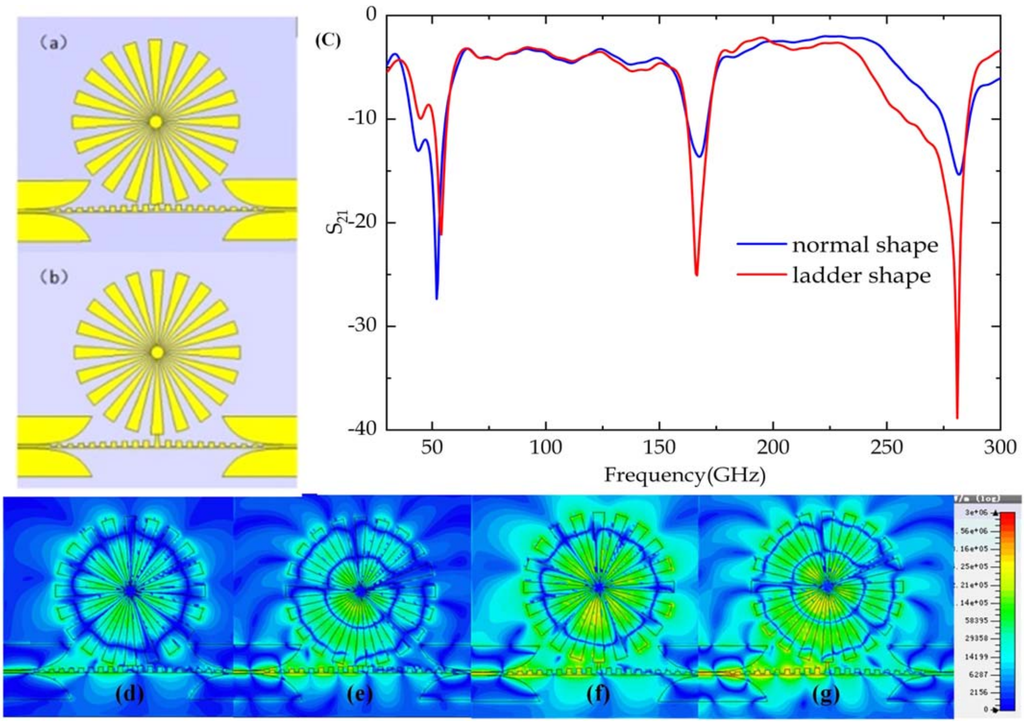

Fig. 4. (Color online) The differences in S_{21} between the normal shape and the ladder shape of the plasmonic chip and the electric field distribution in the second-order and third-order modes of the normal shape; the electric field distribution in (d) the second-order radial modes of the normal shape; (e) the third-order radial modes of the normal shape; (f) the second-order radial modes of the ladder shape; and (g) the third-order radial modes of the ladder shape.

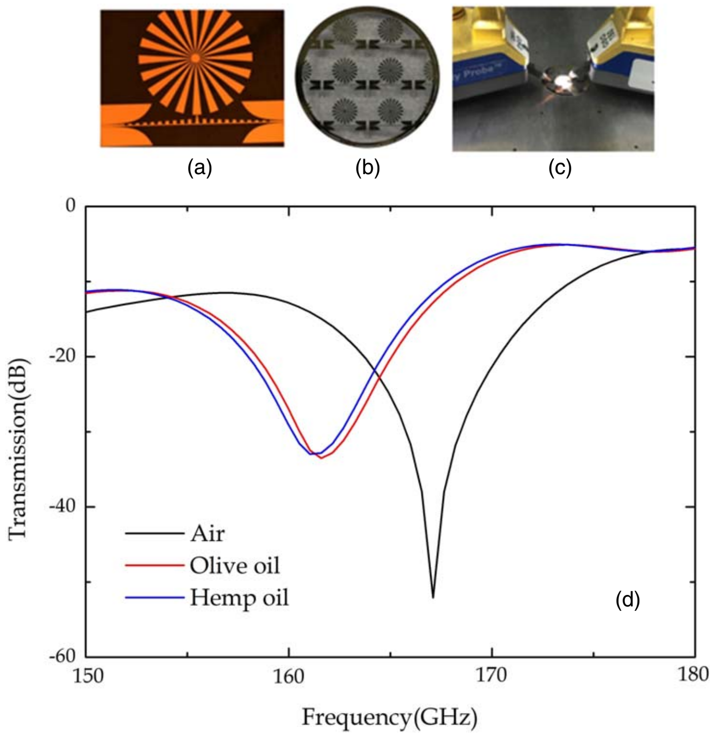

Fig. 5. (Color online) The proposed sensing chip: (a) microscope image, (b) wafer, (c) measurement platform, (d) experimental results of second-order radial mode with different oils.

using a ladder-shaped unit, the transmission coefficient S_{21} can drop from -13.6 dB to -25 dB (from -15.3 dB to -38.8 dB) at the resonance frequency of the second (third) radial order spoof LSPs. The reason is that SPPs are very sensitive to small changes in the surface and are likely to be scattered into the air due to sudden changes in the guiding structure. This sudden change acts as an antenna, and reemits THz waves to excite higher radial order spoof LSPs by grazing incidence. To further confirm the advantage of the ladder-shaped unit, the electric field distributions at 166.5 GHz [Fig. 4(d) (normal shape), 4(f) (ladder shape)] and 280.5 GHz [Fig. 4(e) (normal shape), 4(g) (ladder shape)] are plotted. Comparing the normal shape with the ladder shape, the ladder-shaped metallic unit actually serves as a scatterer which can enhance the excitation of the higher radial order spoof LSPs and cause larger Q values compared to the normal structure.

A plasmonic sensing chip sample is shown in Fig. 5. The thickness of the quartz substrate is 1 cm. The sensing chip is fabricated by using the conventional lithography method. When the sample is ready, we measure the transmission coefficient S_{21} by an Agilent N5245A vector network analyzer using the WR5.1 module (140–220 GHz, covering the second-order radial modes). As shown in Fig. 5(c), two probe pins are placed at port in and out to introduce and detect terahertz signals from the VDI module. The transmission spectra of the second-order modes with olive oil, with hemp oil and without oil are shown in Fig. 5(d). A difference in refraction index of 0.02 can result in a frequency shift of 0.4 GHz. The experimental results fit well the simulation results. There are also some slight deviations, which are mainly caused by fabrication and measurement tolerances.

In summary, an ultrathin plasmonic sensing chip that can excite higher radial order spoof LSP modes is proposed. Radial fundamental, second-order and third-order modes of the spoof LSPs can be found in the transmission spectra and can be verified by analyzing the dispersion relation and electric field profiles. We also demonstrate that the sensitivity of higher-order modes is proportional to the fundamental order by measuring the frequency shift of edible oils. For example, the sensitivity of the radial third order is nine times that of the radial fundamental order. This proves that the higher the order, the higher the sensitivity. The proposed plasmonic sensing chip has potential applications in biosensing at the THz band.

Acknowledgments This project was supported by the National Key R&D Program of China (2016YFF0100503, 2018YFF01013003), a program of the Shanghai Pujiang Program, China (No. 17PJD028), the National Natural Science Foundation of China (Nos. 61671302, 61601291, and 61722111), the Shuguang Program supported by the Shanghai Education Development Foundation and the Shanghai Municipal Education Commission, China (No. 18SG44), the 111 Project (D18014), the International Joint Lab Program supported by the Science and Technology Commission Shanghai Municipality (17590750300), and the Ministry of Science and Higher Education within the state assignment FSRC ≪Crystallography and Photonics≫ RAS. Correspondence should be addressed to Lin Chen (linchen@usst.edu.cn).

ORCID iDs Lin Chen https://orcid.org/0000-0002-6848-5257 Alexey V. Balakin https://orcid.org/0000-0002-3631-3522

1) A. F. Harvey, “Periodic and guiding structures at microwave frequencies,” IRE Trans. Microwave Theory Tech. **8**, 30 (1960).
2) L. Chen, Z. Q. Cao, F. Ou, H. G. Li, Q. S. Shen, and H. C. Qiao, “Observation of large positive and negative lateral shifts of a reflected beam from symmetrical metal-cladding waveguides,” Opt. Lett. **32**, 1432 (2007).
3) A. S Maier, *Plasmonics: Fundamentals and Applications* (Springer, Berlin, 2007) 52, 49.
4) F. J. Garcia-Vidal, L. Martín-Moreno, and J. B. Pendry, “Surfaces with holes in them: new plasmonic metamaterials,” Opt. Pure Appl. Opt. **7**, S97 (2005).
5) J. B. Pendry, L. Martín-Moreno, and F. J. Garcia-Vidal, “Mimicking surface plasmons with structured surfaces,” Science **305**, 847 (2004).
6) A. P. Hibbins, B. R. Evans, and J. R. Sambles, “Experimental verification of designer surface plasmons,” Science **308**, 670 (2005).
7) X. Gao, L. Zhou, Z. Liao, H. F. Ma, and T. J. Cui, “An ultra-wideband surface plasmonic filter in microwave frequency,” Appl. Phys. Lett. **104**, 191603 (2014).
8) S. Laurette, A. Treizebre, and B. Bocquet, “Corrugated Goubau lines to slow down and confine THz waves,” IEEE Trans. Terahertz Sci. Technol. **2**, 340 (2012).
9) A. P. Huidobro et al., “Magnetic localized surface plasmons,” Phys. Rev. X **4**, 340 (2014).
10) A. Pors, E. Moreno, L. Martin-Moreno, J. B. Pendry, and F. J. Garcia-Vidal, “Localized spoof plasmons arise while texturing closed surfaces,” Phys. Rev. Lett. **108**, 223905 (2012).
11) X. Shen and T. J. Cui, “Ultrathin plasmonic metamaterial for spoof localized surface plasmons,” Laser Photonics Rev. **8**, 137 (2014).
12) Z. Liao, Y. Luo, A. I. Fernández-Domínguez, X. P. Shen, A. S. A. Maier, and T. J. Cui:, “High-order localized spoof surface plasmon resonances and experimental verifications,” Sci. Rep. **5**, 9590 (2015).
13) L. Chen, Y. M. Wei, X. F. Zang, Y. M. Zhu, and S. L. Zhuang, “Excitation of dark multipolar plasmonic resonances at terahertz frequencies,” Sci. Rep. **6**, 22027 (2016).
14) L. Chen et al., “Defect-induced Fano resonances in corrugated plasmonic metamaterials,” Adv. Opt. Mater. **5**, 1600960 (2017).
15) K. B. Crozier, A. Sundaramurthy, G. S. Kino, and C. F. Quate, “Optical antennas: resonators for local field enhancement,” J. Appl. Phys. **94**, 4632 (2003).
16) Z. J. Ma et al., “Terahertz particle-in-liquid sensing with spoof surface plasmon polariton waveguides,” APL Photonics **2**, 116102 (2017).
17) J. J. Yang, F. Yan, and D. Z. Chen, “Broadband molecular sensing with a tapered spoof plasmon waveguide,” Opt. Express **23**, 8583 (2015).
18) L. Chen, D. Liao, X. Guo, J. Zhao, Y. Zhu, and S. Zhuang, “Terahertz time-domain spectroscopy and micro-cavity components for probing samples: a review,” Frontiers Inf. Technol. Electron. Eng. **20**, 591 (2019).
19) J. N. Anker et al., “Biosensing with plasmonic nanosensors,” Nat. Mater. **7**, 442 (2008).
20) H. Z. Yao, S. C. Zhong, and W. L. Tu, “Performance analysis of higher mode spoof surface plasmon polariton for terahertz sensing,” J. Appl. Phys. **117**, 133104 (2015).
21) X. Y. Liu, Y. J. Feng, B. Zhu, J. M. Zhao, and T. Jiang, “High-order modes of spoof surface plasmonic wave transmission on thin metal film structure,” Opt. Express **21**, 31155 (2013).
22) T. Jiang, L. Shen, X. Zhang, and L. Ran, “High-order modes of spoof surface plasmon polariton on the periodically corrugated metal surfaces,” Prog. Electromagn. Res. M **8**, 91 (2009).
23) H. Z. Yao and S. C. Zhong, “High-mode spoof SPP of periodic metal grooves for ultra-sensitive terahertz sensing,” Opt. Express **22**, 25149 (2014).
24) D. K. Lee, J. H. Kang, J. S. Lee, H. S. Kim, C. Kim, J. H. Kim, T. Lee, J. H. Son, Q. Park, and M. Seo, “Highly sensitive and selective sugar detection by terahertz nano-antennas,” Sci. Rep. **5**, 15459 (2015).
25) R. Singh, W. Cao, I. Al-Naib, L. Cong, W. Withayachumnankul, and W. Zhang, “Ultrasensitive THz sensing with high-Q Fano resonances in metasurfaces,” Appl. Phys. Lett. **105**, 171101 (2014).
26) D. N. Wang, L. Chen, B. Fang, and Y. M. Zhu, “Spoof localized surface plasmons excited by plasmonic waveguide chip with corrugated disk resonator,” Plasmonics **12**, 947 (2017).
27) M. Tobolova and V. Kresalek, “Edible oil comparison by terahertz time domain spectroscopy system Tera OSCAT,” Latest Trends Syst. **I**, 134 (2014).

